Extreme Mechanics Letters 38 (2020) 100748

Contents lists available at ScienceDirect

Extreme Mechanics Letters

journal homepage: www.elsevier.com/locate/eml

Poisson's ratio of two-dimensional hexagonal crystals: A mechanics model study

Chunbo Zhang [a], Ning Wei [b], Enlai Gao [a,*], Qingping Sun [c,*]

[a] Department of Engineering Mechanics, School of Civil Engineering, Wuhan University, Wuhan, Hubei 430072, China
[b] Jiangsu Key Laboratory of Advanced Food Manufacturing Equipment and Technology, Jiangnan University, 214122 Wuxi, China
[c] Department of Mechanical and Aerospace Engineering, The Hong Kong University of Science and Technology, Hong Kong, China

ARTICLE INFO

Article history:
Received 18 January 2020
Received in revised form 11 March 2020
Accepted 20 April 2020
Available online 25 April 2020

Keywords:
Poisson's ratio
2D hexagonal crystals
Regulation strategies
Limits

ABSTRACT

The Poisson's ratio of two-dimensional hexagonal crystals has been widely studied due to its fundamental and fantastic nature. However, the issue involved in the regulation strategy and in the bounds of Poisson's ratio of two-dimensional hexagonal crystals has not been addressed. In this work, we predict that the Poisson's ratio of two-dimensional hexagonal crystals can be controlled by modifying the structural interaction therein, where the lower bound and upper bound are $-1/3$ and $+1$, respectively. Furthermore, molecular simulations verify these predictions. Finally, the underlying mechanism is revealed as the interplay between two deformation modes (i.e., bond stretching and angle changing). This work provides an universal regulation strategy to tune the Poisson's ratio of two-dimensional hexagonal crystals, and determines fundamental limits on the Poisson's ratio of two-dimensional hexagonal crystals.

1. Introduction

Poisson's ratio, as one of the most fundamental parameters to measure the deformation of materials, has attracted considerable interests [1,2]. Poisson's ratio not only affects the elastic behaviors of materials, but also closely relates to the material properties beyond elasticity, such as vibration absorption [3], indentation resistance [4], and toughness [5]. Therefore, a large number of strategies including modifying the internal factors, such as the geometry, topology, or anisotropy, and applying external fields, such as temperature, pressure, or electric field, that could control the sign and magnitude of Poisson's ratio have been proposed [1,2,6]. The limits on the Poisson's ratio of conventional three-dimensional (3D) isotropic materials are well known as $-1 < \nu < 1/2$ that results from the requirement of elastic stability. As the compressibility increases, the Poisson's ratio of 3D isotropic materials decreases from 1/2 to -1. To be specific, for highly incompressible rubber, $\nu \approx 0.5$; for slightly compressible metals, polymers and ceramics, $0.25 < \nu < 0.35$; for more compressible network structures, ν can be negative; for highly compressible fluids, ν can even approach -1 [1]. In addition to isotropic materials, Ting et al. predicted that the Poisson's ratio for anisotropic materials has no bounds [7]. These studies on the regulation strategies and the bounds of the Poisson's ratio are of fundamental importance for guiding the design, fabrication, and applications of 3D materials having diverse Poisson's ratios.

Recently two-dimensional (2D) materials have received much attention because of their extraordinary properties resulting from the reduced dimensions [8–14]. Most of 2D materials possess hexagonal lattice [15] and thus are named as two-dimensional hexagonal crystals (2DHCs), in which the well-known examples are graphene and hexagonal boron nitride (*h*-BN). The in-plane elastic behavior of 2DHCs is known as elastic isotropy resulting from their six-fold rotational symmetry [16]. Thus it calls for only two independent elastic constants to measure the elastic deformation, in which the Poisson's ratio is a commonly used one. Many studies have been conducted to investigate the Poisson's ratios of 2DHCs, and thus diverse Poisson's behaviors have been observed in 2D materials by tailoring their structures, such as introducing ripples, hydrogenation, or free edges [17–21]. Grima et al. demonstrated that graphene can be modified to exhibit a negative Poisson's ratio by introducing defects, which was explained by a 'crumpled paper' model [17]. Subsequently, it was further shown that graphene can exhibit a large magnitude of negative Poisson's ratio by distributing defects in a specific arrangement [19]. Wan et al. found that the Poisson's ratio of monolayer graphene oxide can be controlled from positive to negative values by modifying its oxidation degree [21]. Furthermore, Jiang et al. found that graphene can exhibit negative Poisson's ratio in a certain stage of the strain–stress curve resulting from the interplay of atom interactions [22]. The Poisson's ratios, especially negative Poisson's ratios of 2DHCs have been widely studied,

* Corresponding authors.
E-mail addresses: enlaigao@whu.edu.cn (E. Gao), meqpsun@ust.hk (Q. Sun).

https://doi.org/10.1016/j.eml.2020.100748
2352-4316/

while an universal regulation strategy as well as fundamental bounds of the Poisson's ratio of 2DHCs has not been determined.

In this work, we predict that the Poisson's ratio of 2DHCs can decrease from $+1$ to $-1/3$ by increasing the ratio between angle stiffness and bond stiffness of 2DHCs. Subsequently, molecular simulations are performed to verify this prediction. Finally, two deformation modes are proposed to understand the Poisson's behaviors of 2DHCs.

2. Method

We perform molecular simulations by using large-scale atomic/molecular massively parallel simulator (LAMMPS) [23]. The strain energy in 2DHCs consists of V_b (due to bond stretching $(d - d_0)$) and V_a (due to angle change $(\theta - \theta_0)$), where $V_b = k_b\ (d\text{-}d_0)^2$ and $V_a = k_\theta\ (\theta - \theta_0)^2$, respectively. Here d_0, θ_0, k_b and k_θ are the equilibrium bond length, equilibrium angle, bond stiffness and angle stiffness, respectively. It is worth mentioning here that the out-of-plane deformation also plays an essential role in the mechanical properties of 2DHCs. However, the out-of-plane elasticity is characterized by an independent elastic constant, i.e., angle stiffness of 2DHCs, which only correlates to the stiffness of dihedral angle in the bead–spring model [24]. Hence, the out-of-plane deformation is independent from the in-plane bond stretching, angle changing and Poisson's ratio. Considering these facts, out-of-plane deformation is not considered in investigating the in-plane Poisson's behaviors of the 2DHCs. Without loss generality, unitless simulations are performed and the fundamental quantities of length and energy are set as σ and ε, respectively. Herein d_0 and k_b are adopted as 1σ and $1\varepsilon/\sigma^2$, respectively. To explore the effect of $\lambda = \frac{k_\theta}{k_b d_0^2}$ that characterizes the ratio of mechanical resistance between angle and bond deformation on the mechanical behavior of 2DHC, k_θ is adopted as $\lambda\varepsilon$, where λ is modified in simulations. Furthermore, a $2\times2\times1$ supercell of 2DHCs is modeled (Fig. 1a). To avoid the size effect of the model, periodic boundary conditions are applied in the in-plane directions. Before the tensile deformation is applied, the sheet of 2DHC is energetically minimized by using conjugate gradient algorithm. To investigate the mechanical behaviors of 2DHCs with different λ, we perform tensile and shear tests on 2DHCs. To be specific, in the tensile test, tensile strain with increment of 0.5% per step until 5% along x (y) direction is applied, while the freedom of the structure in y (x) direction is relaxed to minimize the system energy. In the shear test, shear strain with increment of 0.5% per step until 5% along x (y) direction is realized by tilting the box.

3. Results and discussion

3.1. Theoretical prediction

For 2DHCs subjected to in-plane deformation, the material deformation can be mapped into the change of bonds and angles. By using this method, Gillis et al. related the material elastic properties to the bond and angle interaction of 2DHCs [25], which was used to describe the elastic responses of graphene [26] and other 2DHCs [24]. As illustrated in Fig. 1a, the equilibrium bond length and angle are defined as d_0 and θ_0, respectively, and the bond stiffness k_b and angle stiffness k_θ determine the resistance of bond stretching and angle changing, respectively. When a tensile force is applied on the periodic unit of 2DHCs (Fig. 1b), the lateral strain of ε_x and applied strain of ε_y can be related to the deformation of bonds and angles in 2DHCs. To be specific, by applying a force f along the bond between two atoms, the bond length change is $d - d_0$, which is described as

$$f = k_b(d - d_0) \tag{1}$$

Similarly, as a torque T is applied between a pair of connected bonds, the induced change of angle is θ-θ_0. The relation between them can be written as

$$T = k_\theta(\theta - \theta_0) \tag{2}$$

where θ_0 equals 120° in 2DHCs. Considering a tensile force is applied on the periodic unit of 2DHCs as shown in Fig. 1b, the deformation can be mapped into the change of three bonds and three angles. The force acting on the bonds of B_1 (B_2) can be decomposed into two components along and perpendicular to the bond as $f_1 = F\sin 30°$ and $f_2 = F\cos 30°$, respectively. Thus, the bonds of B_1, B_2 and B_3 yield the displacement of f_1/k_b, f_1/k_b, and $2F/k_b$ along bond stretching direction, respectively. The displacement of B_2 ($\Delta d_1 = f_1/k_b$) induced by f_1 can be decomposed into two components along the x and y directions as $\Delta d_1 \cos 30°$ and $\Delta d_1 \sin 30°$, respectively. Meanwhile, bonds of B_1 and B_2 also yield angle deformation resulting from f_2. Considering the cooperative effect in the deformation of angle, the angle change ($\angle$AOD) can be calculated as

$$\Delta\theta = f_2 d_0/3k_\theta \tag{3}$$

Thus the displacement of B_2 induced by f_2 is

$$\Delta d_2 = d_0\Delta\theta/2 \tag{4}$$

which can be decomposed into two components along x and y directions as $-\Delta d_2 \sin 30°$ and $\Delta d_2 \cos 30°$, respectively. Hence, the displacements along the x and y directions are calculated as the sum of the corresponding components of the bond stretching and angle changing as

$$\Delta x = 2(\Delta d_1 \cos 30° - \Delta d_2 \sin 30°) \tag{5}$$

$$\Delta y = \Delta d_1 \sin 30° + \Delta d_2 \cos 30° + 2F/k_b \tag{6}$$

The corresponding strains $\varepsilon_x = \Delta x/(\sqrt{3}d_0)$ and $\varepsilon_y = \Delta y/(3d_0/2)$ are

$$\varepsilon_x = (F/12d_0)(6/k_b - d_0^2/k_\theta) \tag{7}$$

$$\varepsilon_y = (F/12d_0)(18/k_b + d_0^2/k_\theta) \tag{8}$$

Combining Eqs. (7)–(8), the Poisson's ratio of 2DHCs can be derived as

$$\upsilon = \frac{(1\text{–}6\lambda)}{18\lambda + 1} \tag{9}$$

where we define a dimensionless factor $\lambda = \frac{k_\theta}{k_b d_0^2}$, which characterizes the ratio of mechanical resistance between angle and bond deformation. Similarly, this formula can be also derived when the tensile force is applied in x direction (See Supplemental Material for details). The bond and angle stiffness should be positive ($\lambda > 0$) from the requirement of elastic stability of 2DHCs. Thus the range of ν can be derived as

$$-1/3 < \nu < 1 \tag{10}$$

It can be found that ν increases from $-1/3$ to $+1$ with the decreasing of λ. As an evidence, Chang et al. [27] have proposed an analytical model to relate the elastic properties of a single-walled carbon nanotube to its atomic structure, and the bound of $[-1/3, 1]$ can be also concluded from the theoretical formula. In addition, the in-plane Poisson's ratio (ν), Young's modulus (E) and shear modulus (G) of 2DHCs should meet

$$E = 2G(1 + \nu) \tag{11}$$

which results from their in-plane elastic isotropy due to the 6-fold rotational symmetry [16].

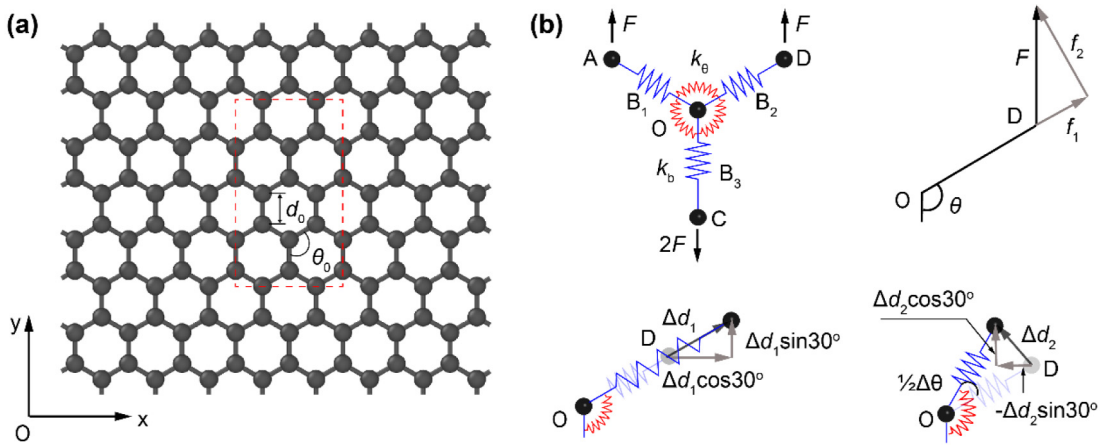

Fig. 1. (a) Illustration of the bead–spring model of 2DHCs. (b) Periodic unit of 2DHCs as stretched along armchair direction. The applied force F is decomposed into two components (f_1 and f_2) along and perpendicular to the bond stretching direction, respectively. The displacement Δd_1 (Δd_2) induced by f_1 (f_2) is further decomposed into two components along the x and y directions, respectively.

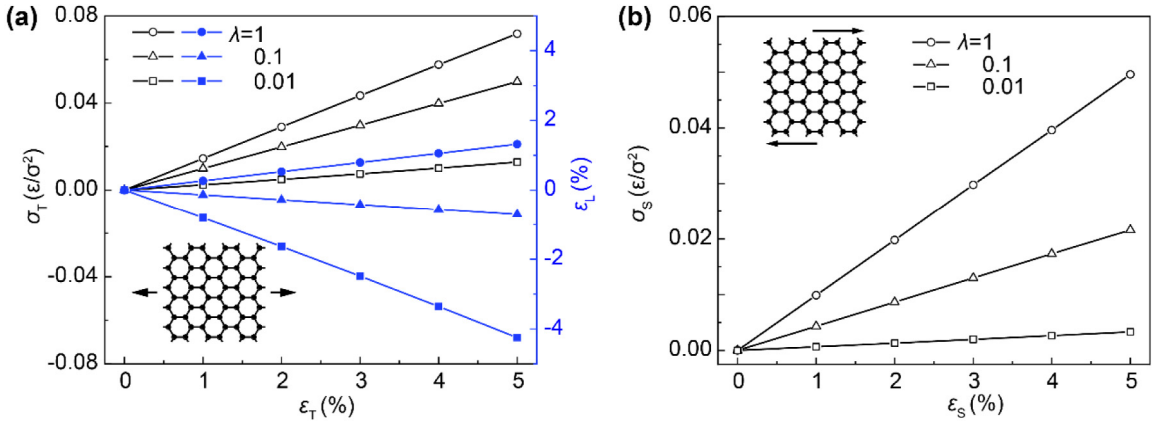

Fig. 2. (a) Tensile stress (σ_T) and lateral strain (ε_L) as the function of tensile strain (ε_T) when uniaxially stretching the periodic unit of 2DHCs along armchair direction. (b) Shear stress (σ_S) as the function of shear strain (ε_S) when shearing the periodic unit of 2DHCs along armchair direction.

It is worth mentioning that the dimensionless factors (λ) of real 2DHCs can be derived from their Poisson's ratios by using the present theoretical formula (Eq. (9)). For example, λ of graphene (0.098), h-BN (0.081) and MoS_2 (0.061) are calculated from the Poisson's ratios of graphene (0.15), h-BN (0.21) and MoS_2 (0.30) [9]. It can be concluded from Eqs. (9) and (11) that the ratio between the resistance against angle changing (shear deformation) and that against bond stretching (tensile deformation) of graphene is larger than that of h-BN as well as MoS_2.

3.2. Molecular simulation

To verify the elastic properties of 2DHCs predicted from theory, we perform tensile and shear tests by using molecular simulations. In these simulations, λ is controlled by modifying the value of angle stiffness (k_θ) while keeping bond stiffness (k_b) constant (See method for details). It should be noted that to avoid defining the controversial thickness of 2D crystals, the 2D stress is used by rescaling the stress with respect to vacuum padding in simulations without loss of generality. The 2D tensile stress (σ_T) and lateral strain (ε_L) as the function of tensile strain (ε_T) in the tensile test, and the 2D shear stress (σ_S) as the function of shear strain (ε_S) in the shear test are recorded, respectively. As 2DHCs tested along armchair direction, both the slopes of strain-stress curves (ε_T-σ_T and ε_S-σ_S) in the tensile and shear tests increase with the increasing of angle stiffness, signifying the increasing of Young's and shear moduli of 2DHCs, respectively, while the slope of ε_L-ε_T in the tensile test decreases with the increasing of angle stiffness, indicating the decreasing of Poisson's ratio of 2DHCs (Fig. 2a–b). These behaviors are also observed in 2DHCs that are tested along zigzag direction (Fig. 3a–b). Furthermore, we extract the Young's modulus, Poisson's ratio and shear modulus from these tensile and shear tests. The simulated relation between them agrees with Eq. (11), consistent with the in-plane elastic isotropy of 2DHCs (Fig. 4).

Furthermore, to verify the regulation strategy as well as the limits on Poisson's ratios for 2DHCs predicated by Eqs. (9)–(10), we calculated ν of 2DHCs having different λ as uniaxially stretched along armchair and zigzag directions. The molecular simulation results demonstrate that with the decrease of the ratio between angle stiffness and bond stiffness, the Poisson's ratios can be tuned from negative to positive values. Additionally, the calculated Poisson's ratios lie between -0.34 and $+1.00$, which agrees with the prediction of the bounds of $-1/3$ and $+1$ for the Poisson's ratio of 2DHCs (Fig. 5a). It demonstrates that λ can be regarded as an univeraial factor to control the sign and magnitude of the Poisson's ratio for 2DHCs under fundamental limits. Considering that λ intrinsically results from the charge density distribution of 2DHCs, the strategies of exciting intrinsic electrons, injecting extrinsic charges, and applying external fields that could modulate the charge density distribution are suggested to manipulate λ in experiments.

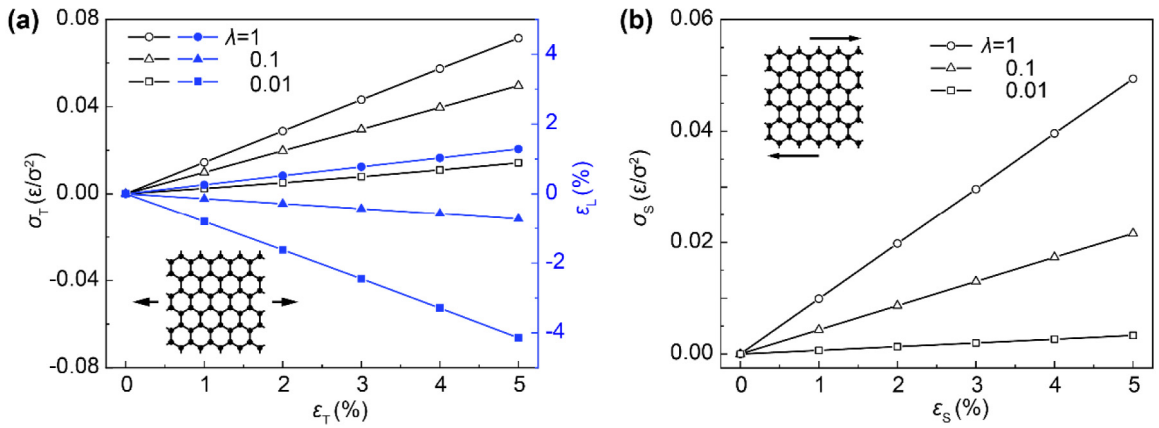

Fig. 3. (a) Tensile stress (σ_T) and lateral strain (ε_L) as the function of tensile strain (ε_T) when uniaxially stretching the periodic unit of 2DHCs along zigzag direction. (b) Shear stress (σ_S) as the function of shear strain (ε_S) when shearing the periodic unit of 2DHCs along zigzag direction.

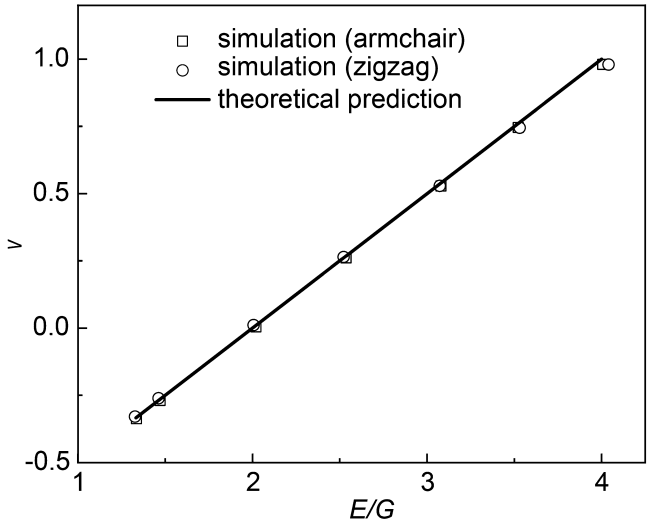

Fig. 4. Relation between Poisson's ratio (ν) and the ratio between Young's modulus and shear modulus (E/G) of 2DHCs as compared between molecular simulation and theoretical prediction (Eq. (11)).

Finally, the underlying mechanism of the abovementioned Poisson's behaviors is revealed from the structural analysis of 2DHCs. Without loss of generality, we take a periodic unit of 2DHCs uniaxially stretched along the armchair direction as an example. As illustrated in Fig. 5b, there are two deformation modes of bond stretching and angle changing, as well as their interacton, which has been used for the understanding of the Poisson's behaviors of graphene [22]. On the one hand, as λ is towards infinity, the bond stretching would dominate the deformation of 2DHCs. Thus all bonds are stretched while the angles almost remain constant in this deformation mode, resulting the lower bound of Poisson's ratio for 2DHCs (−1/3). On the other hand, as λ approaches 0, the angle change dominates the deformation of 2DHCs. Thus the angles would deform while the bond stretching can be neglected in this deformation mode, resulting in the upper bound of Poisson's ratio for 2DHCs (+1). Other Poisson's behaviors of 2DHCs would fall between the two extremes, which could be controlled by modifying the contribution from two deformation modes in 2DHCs.

4. Conclusion and remarks

In summary, we predict that the Poisson's ratio of 2DHCs can be tuned from the lower bound (−1/3) to the upper bound (+1) by modifying the bond and angle stiffnesses in their structures.

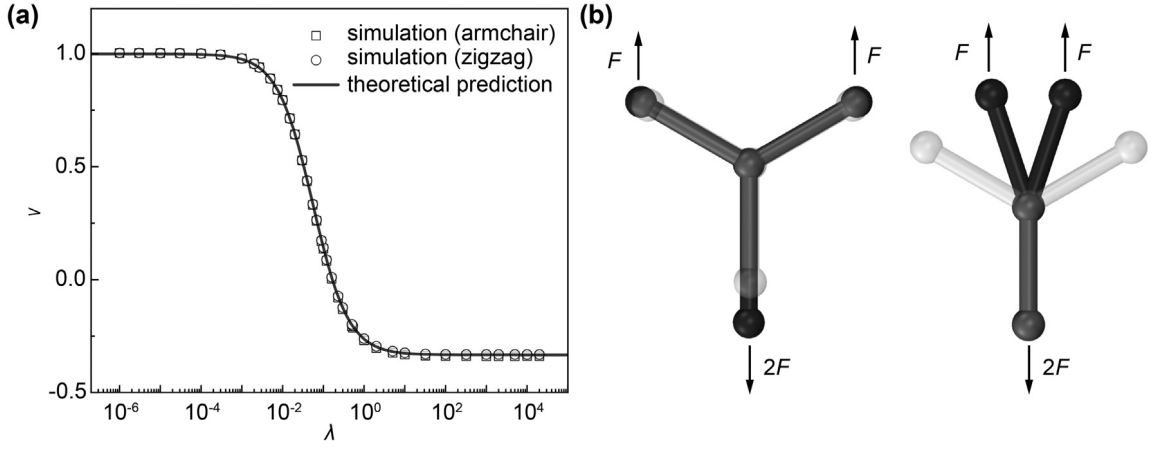

Fig. 5. (a) Relationship between the Poisson's ratio (ν) and the dimensionless factor (λ). The theoretical prediction is from Eq. (9), and the square and circle points are from uniaxial tensile tests along armchair and zigzag directions, respectively. (b) Illustration of two deformation modes of 2DHCs having different λ when applied tensile force: (1) bond-stretching-dominated mode, where angles almost remain constant so the bond stretching dominates the deformation, signifying lower bound of Poisson's ratio (−1/3); (2) angle-changing-dominated mode, where bond lengths almost keep unchanged so angle changing dominates the deformation, signifying upper bound of Poisson's ratio (+1). The gray and black structures represent the initial and deformed configurations, respectively.

Subsequently, the predicted bounds as well as the regulation strategy of Poisson's ratio of 2DHCs are consitent with the molecular simulations. Our findings provide a guidance to design and fabricate 2DHCs exhibiting different Poisson's ratios for diverse applications.

Finally, it is remarked here that the bead–spring model can be generalized into modeling of nonplanar 2DHCs. For example, nonplanar silicene and MoS_2 have been coarse-grained as the bead–spring models by conforming their mechanical properties [24]. Hence, the Poisson's behaviors of nonplanar 2DHCs are expected to be captured by the presented theory if they can be coarse-grained as the bead–spring model of 2DHCs. However, it is noted that the topology, geometry as well as the interaction defined in this work is just an ideal model of 2DHCs that have complex electron charge density distribution in reality. Considering these facts, the Poisson's behavior of 2DHCs maybe much more diverse in reality. To uncover new Poisson's behavior of 2DHCs beyond this work, data-mining of the Poisson's ratio of 2DHCs based on first principles calculations will be one of the promising ways, and can be explored in the future work.

Declaration of competing interest

The authors declare that they have no known competing financial interests or personal relationships that could have appeared to influence the work reported in this paper.

Acknowledgments

This work was supported by the National Natural Science Foundation of China (11902225), the Natural Science Foundation of Hubei Province, China (2019CFB174), the Fundamental Research Funds for the Central Universities, China (413000091), and the Starting-up Fund of Wuhan University, China. The numerical calculations in this work have been done on the supercomputing system in the Supercomputing Center of Wuhan University. C.Z. acknowledges the technical advices from Xiangzheng Jia.

Appendix A. Supplementary data

Supplementary material related to this article can be found online at https://doi.org/10.1016/j.eml.2020.100748.

References

[1] G.N. Greaves, A.L. Greer, R.S. Lakes, T. Rouxel, Nature Mater. 10 (2011) 823.
[2] C. Huang, L. Chen, Adv. Mater. 28 (2016) 8079.
[3] A.W. Lipsett, A.I. Beltzer, J. Acoust. Soc. Am. 84 (1988) 2179.
[4] R.S. Lakes, K. Elms, J. Compos. Mater. 27 (2016) 1193.
[5] J.B. Choi, R.S. Lakes, Int. J. Fract. 80 (1996) 73.
[6] Y. Wen, E. Gao, Z. Hu, T. Xu, H. Lu, Z. Xu, C. Li, Nature Commun. 10 (2019) 2446.
[7] T.C.T. Ting, T.Y. Chen, Q. J. Mech. Appl. Math. 58 (2005) 73.
[8] K.S. Novoselov, A.K. Geim, S.V. Morozov, D. Jiang, Y. Zhang, S.V. Dubonos, I.V. Grigorieva, A.A. Firsov, Science 306 (2004) 666.
[9] E.L. Gao, Z.P. Xu, J. Appl. Mech. 82 (2015) 121012.
[10] R. Li, Q. Shao, E. Gao, Z. Liu, Extreme Mech. Lett. 34 (2020) 100615.
[11] Z.G. Song, Z.P. Xu, Extreme Mech. Lett. 6 (2016) 82.
[12] D. Akinwande, C.J. Brennan, J.S. Bunch, P. Egberts, J.R. Felts, H. Gao, R. Huang, J.-S. Kim, T. Li, Y. Li, K.M. Liechti, N. Lu, H.S. Park, E.J. Reed, P. Wang, B.I. Yakobson, T. Zhang, Y.-W. Zhang, Y. Zhou, Y. Zhu, Extreme Mech. Lett. 13 (2017) 42.
[13] X. Jia, Z. Liu, E. Gao, NPJ Comput. Mater. 6 (2020) 13, http://dx.doi.org/10.1038/s41524-020-0279-8.
[14] E. Gao, B. Xie, Z. Xu, J. Appl. Phys. 119 (2016) 014301.
[15] H. Ding, Z. Zhen, H. Imtiaz, W. Guo, H. Zhu, B. Liu, Extreme Mech. Lett. 32 (2019) 100507.
[16] J.F. Nye, Physical Properties of Crystals: Their Representation By Tensors and Matrices, Clarendon Press, 1957.
[17] J.N. Grima, S. Winczewski, L. Mizzi, M.C. Grech, R. Cauchi, R. Gatt, D. Attard, K.W. Wojciechowski, J. Rybicki, Adv. Mater. 27 (2015) 1455.
[18] J.W. Jiang, H.S. Park, Nano Lett. 16 (2016) 2657.
[19] J.N. Grima, M.C. Grech, J.N. Grima-Cornish, R. Gatt, D. Attard, D, Ann. Phys. 530 (2018) 170033.
[20] J.W. Jiang, T. Chang, X. Guo, Nanoscale 8 (2016) 15948.
[21] J. Wan, J.W. Jiang, H.S. Park, Nanoscale 9 (2017) 4007.
[22] J.W. Jiang, T. Chang, X. Guo, H.S. Park, Nano Lett. 16 (2016) 5286.
[23] S. Plimpton, J. Comput. Phys. 117 (1995) 1.
[24] E.L. Gao, S.Z. Lin, Z. Qin, M.J. Buehler, X.Q. Feng, Z.P. Xu, J. Mech. Phys. Solids 115 (2018) 248.
[25] P.P. Gillis, Carbon 22 (1984) 387.
[26] L. Ruiz, W.J. Xia, Z.X. Meng, S. Keten, Carbon 82 (2015) 103.
[27] T. Chang, H. Gao, J. Mech. Phys. Solids 51 (2003) 1059.

Supplemental Material for

Poisson's Ratio of Two-Dimensional Hexagonal Crystals: A Mechanics Model Study

Chunbo Zhang[1], Ning Wei[2], Enlai Gao[1*] and Qingping Sun[3*]

[1]Department of Engineering Mechanics, School of Civil Engineering, Wuhan University, Wuhan, Hubei 430072, China.

[2]Jiangsu Key Laboratory of Advanced Food Manufacturing Equipment and Technology, Jiangnan University, 214122 Wuxi, China.

[3]Department of Mechanical and Aerospace Engineering, The Hong Kong University of Science and Technology, Hong Kong, China.

[*]Corresponding author. Email: enlaigao@whu.edu.cn; meqpsun@ust.hk;

Theoretical derivation based on the force applied in the zigzag direction.

When the tensile load is applied in *x* direction (**Fig. S1**), the force acting on the bonds of B_1 (B_2) can be decomposed into two components along and perpendicular to the bond as $f_1 = F\cos30^o$ and $f_2 = F\sin30^o$, respectively. Thus, the bonds of B_1 and B_2 yield the displacement of f_1/k_b and f_1/k_b along bond stretching direction, respectively. The displacement of B_2 ($\Delta d_1 = f_1/k_b$) induced by f_1 can be decomposed into two components along the *x* and *y* directions as $\Delta d_1\cos30^o$ and $\Delta d_1\sin30^o$, respectively. Meanwhile, bonds of B_1 and B_2 also yield bending deformation resulting from f_2. Considering the cooperative effect in the deformation of angle, the angle change ($\angle$AOD) can be calculated as

$$\Delta\theta = f_2 d_0/3k_\theta \tag{S1}$$

Thus the displacement of B_2 induced by f_2 is

$$\Delta d_2 = d_0\Delta\theta/2 \tag{S2}$$

which can be decomposed into two components along *x* and *y* directions as $\Delta d_2\sin30^o$ and $-\Delta d_2\cos30^o$, respectively. Hence, the displacements along the *x* and *y* directions are calculated as the sum of the corresponding components of the bond stretching and angle bending as

$$\Delta x = 2(\Delta d_1\cos30^o + \Delta d_2\sin30^o) \tag{S3}$$

$$\Delta y = \Delta d_1\sin30^o - \Delta d_2\cos30^o \tag{S4}$$

The corresponding strains $\varepsilon_x = \Delta x/(\sqrt{3}d_0)$ and $\varepsilon_y = \Delta y/(3d_0/2)$ are

$$\varepsilon_x = (F/12\sqrt{3}d_0)(18/k_b + d_0^2/k_\theta) \tag{S5}$$

$$\varepsilon_y = (F/12\sqrt{3}d_0)(18/k_b - d_0^2/k_\theta) \tag{S6}$$

Combining **Eqs. S5-S6**, the Poisson's ratio of 2DHCs can be derived as

$$\upsilon = \frac{(1-6\lambda)}{18\lambda+1} \tag{S7}$$

where $\lambda = \frac{k_\theta}{k_b d_0^2}$ characterizes the ratio of mechanical resistance between angle and bond deformation.'

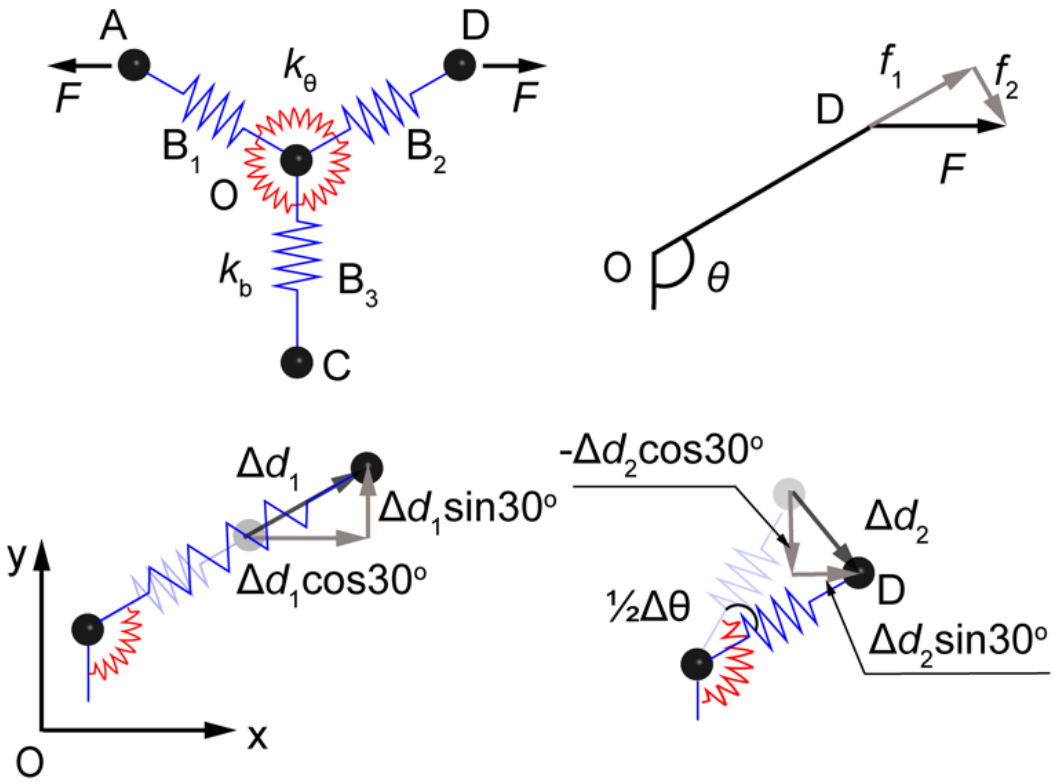

Fig. S1 Periodic unit of 2DHCs as stretched along zigzag direction. The applied force F is decomposed into two components (f_1 and f_2) along and perpendicular to the bond stretching direction, respectively. The displacement Δd_1 (Δd_2) induced by f_1 (f_2) is further decomposed into two components along the x and y directions, respectively.